

UAV Attitude Control using the Visual Horizon

Saul Thurrowgood, Richard J. D. Moore, Daniel Bland, Dean Soccoc and Mandyam V. Srinivasan

University of Queensland, Brisbane, Australia

Abstract

We present a technique for measuring, controlling, and stabilizing the attitude of a UAV by using a camera to monitor the visual horizon. A vision-based algorithm incorporating color and intensity information is used to detect the horizon by segmenting the ground from the sky. The attitude of the aircraft is then measured using the position, shape, and orientation of the horizon profile in the camera image. We show that this information can be used to stabilize the roll and pitch of the aircraft, to achieve and maintain any desired attitude, as well as to orchestrate a number of challenging aerobatic maneuvers that are within the limits of the aircraft's performance envelope.

1 Introduction

The ability to measure, stabilize, and control attitude is critical for any aircraft that is required to fly autonomously. Traditionally, attitude stabilization is achieved using rate gyros to sense and correct unwanted rotations in yaw, pitch, and roll [Rohac, 2005]. While this method is a standard feature of many autopilot systems, it is susceptible to drift during long duration flights. The reason is that rate gyros only sense angular velocities and not angular position *per se*. Therefore, they do not provide an absolute orientation reference. Instead, the yaw, pitch, and roll of the aircraft must be obtained by integrating the rate signals – a process that can lead to substantial noise-induced drift. Another approach is to use the direction of gravity, as sensed by accelerometers, to estimate and stabilize attitude. But this approach can be compromised when an aircraft makes turns, which generate centripetal forces [Rohac, 2005]. The above shortcomings can be overcome by using sensors that provide direct information on absolute orientation. For example, 3-axis magnetometers, used in combination with gyroscopes

and/or accelerometers, can be used to obtain information about an aircraft's absolute orientation [Merhav, 1996]. However, magnetometers on their own will not sense rotations about an axis that is parallel to the direction of the local magnetic field [Merhav, 1996]. Another way of deriving absolute orientation is to take advantage of the fact that the sky is usually brighter than the ground (in the visible spectrum) or darker than the ground (in the infrared spectrum), and use this to determine which direction is "up". Infrared sensors are a compact, lightweight, and cost-effective means of implementing this technique to stabilize roll and pitch [Jalink *et al.*, 1972; Gwozdecki, 2001]. However, they are susceptible to errors when the sun is low in the sky. Another vision-based method for determining attitude involves capturing a wide-angle view of the environment, including the horizon. The position and orientation of the horizon, obtained after segmenting the image into sky and ground, is used to infer the aircraft's attitude [Cornall *et al.*, 2006; Todorovic *et al.*, 2003; Ettinger *et al.*, 2002]. While this technique is more robust to variations in the sun's position, it can be computationally intensive and challenging to implement in real time because of the sophisticated spectral and intensity analysis that is required to achieve reliable sky/ground segmentation. A related method uses a specially designed VLSI chip to extract horizon information in real time from a photodiode array [Horiuchi, 2005]. While this approach is attractive, its accuracy – at least in its present form – is likely to be limited because it uses only intensity information to locate the horizon.

Here we build on our recent work in developing an efficient and reliable horizon-based attitude sensing algorithm, [Thurrowgood *et al.*, 2009], by implementing this algorithm in an aircraft and measuring its performance in stabilizing the aircraft's attitude in closed-loop flight, as well as orchestrating a number of challenging aerobatic maneuvers.

2 Visual Horizon Detection

The basic operation of any horizon detection system is to divide the image into two classes, one ground and the other sky, and to find the contour that best separates these two classes. The visual horizon detection system used here contains an implementation of the method described in [Thurrowgood *et al.*, 2009]. It comprises four steps which are summarized briefly below.

This work was supported partly by US Army Research Office MURI ARMY-W911NF041076, Technical Monitor Dr Tom Doligalski, US ONR Award N00014-04-1-0334, by an ARC Centre of Excellence Grant CE0561903, and by a Queensland Smart State Premier's Fellowship.

Authors are associated with the Queensland Brain Institute and the School of Information Technology and Electrical Engineering, University of Queensland, St Lucia, QLD 4072, Australia and also ARC Centre of Excellence in Vision Science, Australia (email: s.thurrowgood@uq.edu.au).

2.1 Enhancement of Sky/Ground Contrast

For the purposes of computational efficiency we would like to reduce the *RGB* color space to a 1D axis (here called C) such that the ground and sky pixels can be reliably separated. By analyzing a set of 124 images covering a range of different visual environments such as snow, desert, farm land, and inner city, we have obtained the following transformation that achieves this objective,

$$C = -0.58R + 0.18G + 0.72B + 87. \quad (1)$$

The procedure for finding this transform is detailed in [Thurrowgood *et al.*, 2009]. The idea is to find a plane through color space that well separates the manually tagged sky and ground classes from the training images. We choose a transform that projects colors onto a line perpendicular to that classification plane. This allows us to delay the actual classification until we apply a threshold to the C values of the captured images, giving a single degree of freedom in classification during run-time.

To avoid saturation of 8-bit data, C has been scaled and offset from the original to the range [0,255] which is important for the following histogram analysis. Fig. 1 shows a histogram of C values obtained for all pixels in the same set of 124 images. A threshold is applied to C to determine whether a given pixel belongs to the ground or the sky.

2.2 Determination of Optimum Threshold

Based on the above discussion, the threshold for C is selected by computing a 256-bin histogram of the transformed image pixels, and adopting an approach for threshold selection that incorporates two weighting functions, W_1 and W_2 :

W_1 Higher weight is given to histogram bins with small values, to prefer a threshold at a position with low rate of change of image area with respect to histogram bin.

W_2 Higher weight is given to histogram bins that are near the median value of C for the given image, using a normalized integral of the histogram, to prefer 50:50 area coverage of sky/ground pixels.

The threshold is selected to be at the bin at which the product of the two weights, W_1 and W_2 , is the maximum.

2.3 From Horizon Edges to 3D Directions

Any point that is on an edge between the sky and ground classes is then considered a candidate horizon point. Camera calibration parameters are used to convert pixel coordinates of these horizon candidate points into unit 3D vectors. Each vector is located with its base at the nodal point of the camera, and is directed toward the appropriate point on the horizon edge.

For high altitude flight where the effects of horizon topography are negligible, the horizon vectors should lie in an equatorial plane that passes through the nodal point of the camera, which is at the centre of the viewsphere $[0,0,0]^T$.

2.4 Fitting a Plane in 3D to Horizon Vectors

Next a plane is fitted, in 3D, to the set of horizon vectors using a least-squared-error procedure. The orientation of

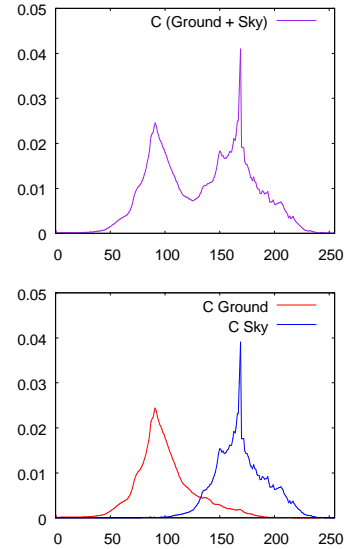


Fig. 1. Top: histogram of C as would be measured for the entire scene of ground plus sky, normalized by the total number of pixels. Bottom: histogram of C plotted separately for the manually classified ground and sky. Classes overlap by 8.6%.

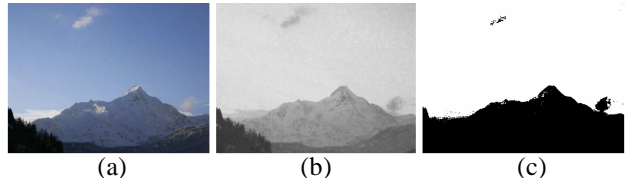


Fig. 2. (a) Original image. (b) Image transformed using (1). (c) Result of applying automatically selected threshold.

this plane relative to the camera's coordinate frame then defines the roll and pitch of the aircraft. Examples of fitted horizon planes, projected back onto the camera images, are shown in Fig. 3, 4, 8 and 12.

A useful property of this method of horizon detection is that it can be “piggybacked” onto any vision system that has been calibrated geometrically, irrespective of the way in which the environment is imaged.

3 Flight Platform

The platform used for the flight tests (Fig. 3, left) is a Super Frontier Senior-46 with a wingspan of 2040mm and a payload capacity of approximately three kilograms. The engine has been relocated to a position above the wings, allowing vision systems to be mounted on the nose with minimal visual obstruction by the aircraft.

3.1 Imaging Systems

The image processing and control system are run onboard the aircraft using a dual-core 1.5GHz PC104 (Digital-Logic MSM-945). Control signals are periodically sent to the control surfaces (in this case only elevator and ailerons) through a microcontroller that allows the human pilot to hand over/take over control to/from the onboard computer. On this computer the horizon image processing runs in under 2.0ms on a single core, while the control system takes negligible time. The majority of processing resources were used to encode and save videos of the image data that formed part of the data log, which was downloaded for post-flight analysis.

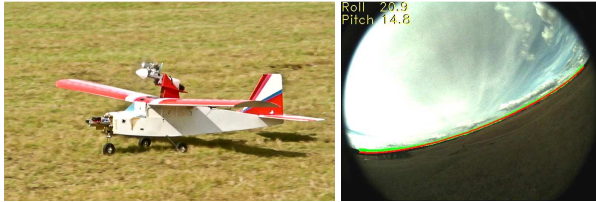


Fig. 3. Vision System A. Left: photo of the aircraft. The camera can be seen as a small black dot mounted on the nose, in front of the black box of the IMU. Right: image captured shortly after takeoff from the fisheye camera on the nose of the aircraft. The estimated horizon, shown in red, is the best planar fit to the candidate horizon points shown in green. The roll and pitch angles (in degrees) correspond to the orientation of the fitted planar surface.

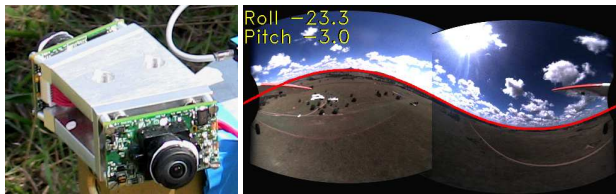


Fig. 4. Vision System B. Left: photo of a dual-fisheye camera system. Right: images captured during flight are stitched together to produce these $360^\circ \times 150^\circ$ FOV images. Again the measured horizon estimate is shown as a red line.

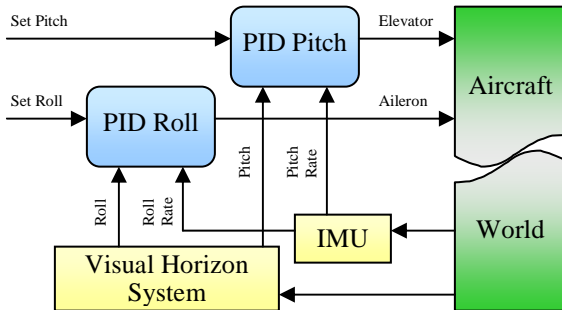


Fig. 5. Diagram of the automatic control system.

The camera chosen for the vision system is a Point Grey Firefly MV which contains a Micron MT9V022 CMOS color sensor capable of a frame rate of 60Hz at the full resolution of 752x480 pixels. Fitted with a Sunex DSL216 lens, the camera provides a 185° field of view (FOV). Due to some cropping of the image circle by the camera sensor, we have a vertical and horizontal FOV of 145° and 185° respectively. We calibrated this camera using the generic camera model in [Kannala and Brandt, 2006]. Two different vision systems were used in this study, as described below.

Vision System A

This setup, shown in Fig. 3, is a single forward-looking camera configured to capture images at 44 Hz. Images were captured at a resolution of 612x480 pixels (which is a cropping of the full 752x480 image to the extent of the image circle) and were scaled down to 306x240 before running the visual attitude measurement algorithm.

Vision System B

This setup, shown in Fig. 4, is a pair of the same cameras configured back-to-back and set to capture stereo images

at 30 Hz. Stereo image pairs were captured at a resolution of 640x480 each and were remapped to a single image with a longitude and latitude mapping of $360^\circ \times 150^\circ$ FOV and a resolution of 360x180 pixels.

3.2 Closed Loop Flight Control

To control the attitude of the aircraft a simple scheme was implemented, comprising a pair of PID control loops, as shown in Fig. 5. The angular attitude is measured by the vision system, while rotational rates are measured using solid state gyros from a Micro-Strain 3DM-GX2 inertial measurement unit (IMU).

3.3 Attitude Reference Frame

The reference frame used for all attitude measures is the calibrated camera model view sphere. The IMU is rigidly mounted and aligned with the camera system. Roll and pitch Euler angles are computed using the “Aircraft” or “ZYX” formulation, but internally we work with attitude as a planar surface described by a 3D vector normal to the plane (the “up” vector).

4 Flight Tests

Four different automatic flights were performed to test the ability of the visual horizon system to control and maintain commanded attitudes during extreme maneuvers. Comparison is also made to the IMU estimate.

4.1 Flight 1: Circular Flight

This flight used Vision System A and, as with all four flights, began with a manually controlled takeoff. After takeoff control was handed over to the onboard computer, which performed all image processing and control. Manual control of the aircraft was then regained, and the aircraft was brought in to land. During the automatic

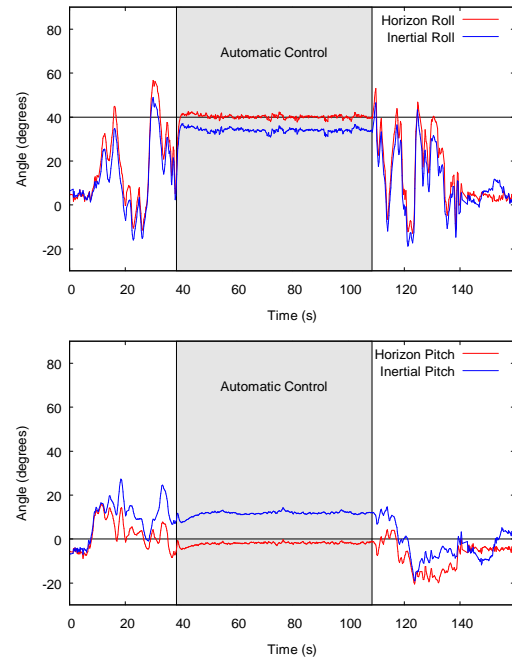


Fig. 6. Estimated attitude of the aircraft relative to the horizon. The 70 second period of automatic control is shaded. Horizontal lines indicate the constant attitude commands. Also plotted is the attitude reported by the IMU.

control phase the set pitch was 0° and the set roll was $+40^\circ$ (rightward roll). The throttle was set to a fixed level, and the rudder was set to zero (straight ahead). This resulted in the aircraft performing clockwise circles, completing approximately three full circuits during automatic control.

Fig. 6 displays the aircraft's roll and pitch angles during the flight test, as measured by the horizon detection algorithm. The entire flight is displayed and the period of automatic flight is highlighted.

During automatic control the mean deviation of roll from the set point was $+0.05^\circ$, with a standard deviation of 1.8° and a mean absolute deviation of 0.82° . The mean deviation of pitch from the set pitch of 0.0° was -2.0° , with a standard deviation of 0.67° .

The results show that the control system was able to attain and hold the requested attitude accurately over the entire period of automatic control. The pitch angle was never attained exactly, partly because of the significant roll angle. The pitch is defined relative to the horizon in this exercise, and is not in the aircraft body frame of reference. Consequently, with increasing aircraft roll, the elevator will cause progressively greater changes in heading, rather than in pitch.

We also see in Fig. 6 that there is a considerable discrepancy between the horizon-based measure and the inertial estimate of attitude, especially with respect to pitch. Note that the IMU was mounted such that it was well aligned with the visual system, as can be seen by their agreement before takeoff and after landing (less than 1° difference). During automatic control, the mean difference between vision and IMU-based roll is -6.1° and for pitch is 13.7° . Visual inspection of the horizon images acquired during the automatic control phase reveals that the aircraft never attained pitch angles as large as even $+10^\circ$ (or greater), as was reported by the IMU. Such large pitch angles would manifest as a distinct concave bend in the horizon when imaged by the fisheye lens.

This result is to be expected since the IMU we are using does not have a direct measure of velocity. The accelerometer readings contain not only the direction of gravity but also components due to centripetal force, which requires a velocity measure to separate the two. So in an extended banked turn we can expect the inertial attitude estimate to diverge from the true value as errors accumulate.

Because the inertial and horizon attitudes both agree while on the ground, and diverge quickly after takeoff, we conclude that the inertial system is suffering from these other acceleration sources, especially once we enter an extended turn. Thus, in terms of a gravity reference system, we see that the horizon-based system of monitoring and controlling attitude outperforms the inertial system in this flight at all times.

4.2 Flight 2: Loop

Flights 2, 3 and 4 used Vision System B. The automatic period of Flight 2 stabilizes the roll of the aircraft to hold the wings level with the horizon (roll angle of 0° or $\pm 180^\circ$), while maintaining the elevator position as full “up” (meaning the setting that produces maximum positive pitch rate). The pitch of the aircraft is monitored by the vision system to detect that the loop has been completed, at which time roll and pitch commands are set to 0° .

Before each of Flights 2, 3 and 4 a simulation

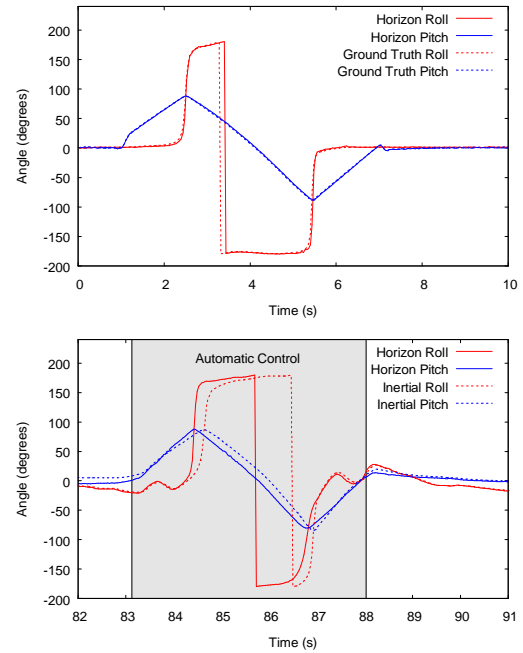


Fig. 7. Top: loop performed in simulation. Bottom: loop performed on actual aircraft.

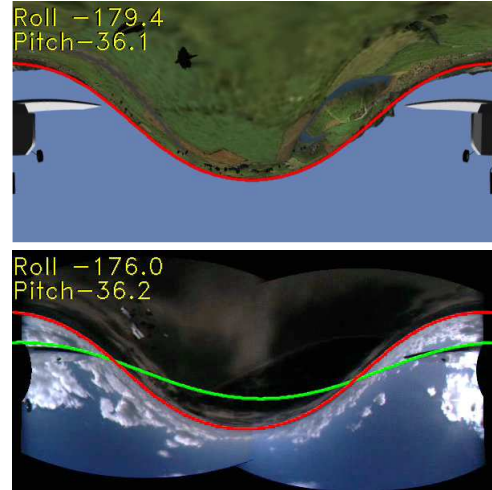


Fig. 8. Images captured during the loop of Flight 2. Top: simulation at time of 4.7 seconds. Bottom: actual flight at time of 86.2 seconds. The red line represents the visual attitude measurement, and the green line the inertial estimate. Note that all maneuvers were performed using lower resolution images (360x180 pixels) in both simulation and on the actual aircraft.

was performed to test the feasibility of these maneuvers, using a 6-DOF aircraft model with dynamics comparable to the actual aircraft. Fig. 7 compares the simulated and the actual aircraft attitudes during the loop and Fig. 8 shows examples of the imagery captured during the same simulated and actual flights. Note that pitch is defined over the range $[-90, +90]^\circ$ while roll is defined over $[-180, +180]^\circ$, and also note that $+180^\circ$ is equal to -180° . There is a good match between simulation and the actual flight for this maneuver, even though the flight dynamics model is not perfectly matched to our aircraft.

During the actual loop we can see that there is oscillation in the roll caused by the proportional gain in the PID controller having been set too high. The profile of

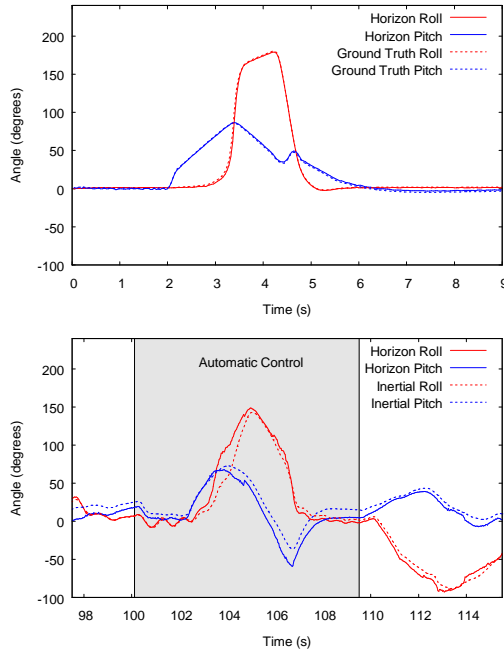


Fig. 9. Top: Immelmann turn performed in simulation. Bottom: Immelmann turn performed on actual aircraft.

the roll angle in the actual flight is not as square as the simulated loop due to the aircraft entering the loop at a non-zero roll angle. We also see that for this maneuver the inertial attitude estimates roughly matched the horizon measurements, though the magnitude of the difference is quite variable over time, with the inertial estimate appearing to lag behind the horizon measure by varying amounts of time.

It can be seen in Fig. 8 that the inertial estimate of pitch does not align well with the horizon, and given the relatively flat landscape, it is not unreasonable to conclude that the inertial estimate is thus not as well aligned with gravity as is the horizon measurement.

4.3 Flight 3: Immelmann Turn

The automatic period of this flight stabilizes the roll in the same way as Flight 2, and the elevator position is again set to full “up”, but the loop is terminated after passing a pitch of $+90^\circ$ and when the pitch comes down to less than $+50^\circ$, at which time the roll and pitch commands are set to 0° . This has the effect of performing a near- 180° turn in heading, with a small increase in height.

The attitude plots for this maneuver are shown in Fig. 9. In this case, the roll attitude when entering the initial loop-like phase of the Immelmann turn is further from zero than in the case of the loop in Flight 2, causing the profile of roll angle in the actual flight to be quite rounded, which corresponds to a trajectory that is rotated away from the vertical, to the right. The other major difference from simulation is in relation to the pitch attitude, which drops much more during the later roll phase of rolling from 180° to 0° , possibly due to the fact that the simulator rolled somewhat faster than the actual aircraft.

Again, the inertial attitude estimates agree roughly with the visual horizon measurements.

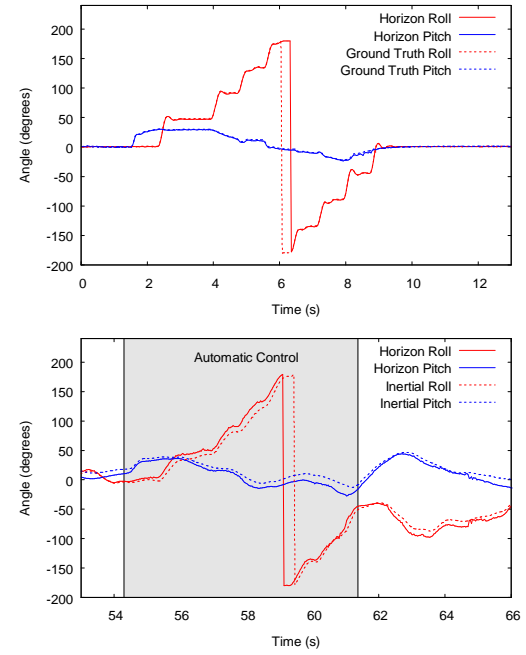


Fig. 10. Top: Stepped roll performed in simulation. Bottom: Stepped roll performed on actual aircraft.

4.4 Flight 4: Stepped Roll

The automatic period of this flight had pitch set to a constant 35° above the horizon, but multiplied by the cosine of roll angle so that there is zero elevator control while banked 90° . This is a consequence of the attitude being relative to an external (horizon) reference frame, rather than the aircraft’s body reference frame. Simultaneously we give a timed change in roll set point. The roll angle is commanded such that the aircraft performs a full 360° roll in steps of 45° . Each commanded roll angle was held for 0.8 seconds.

The actual aircraft performs quite well and close to the simulation (Fig. 10), except for the fact that the real aircraft has a slower response time. In this case the automatic control was aborted prior to the roll angle reaching the final 0° because of proximity to the ground. In these experiments, the control system had no information about height above ground, and this maneuver in particular caused a significant drop in altitude, especially while holding roll angles of $\pm 90^\circ$.

5 Simulation

The simulations for all tested maneuvers show that even when using an image resolution of 360x180 pixels, we can achieve quite accurate measurements of attitude using the visual horizon. Table 1 gives measurements of the angular error between the visual horizon and the ground truth. The angular error is the angle of rotation required to align the measured visual horizon with the ground truth horizontal plane. The major source of error when using simulated imagery is the fact that the simulation includes mountains, trees and buildings, so the visual horizon does not always conform to the idealized horizontal plane that would form a great circle within the view sphere.

	Mean	Std. Dev.	Maximum
Loop	1.2	0.57	2.2
Immelmann Turn	1.5	0.55	2.3
Stepped Roll	1.2	0.65	5.4

Table 1. Angular error of the visual horizon during the simulated maneuvers, in units of degrees.

Further simulations were performed to demonstrate the requirement for continual active control of the aircraft during these maneuvers. Fig. 11 shows the same maneuvers as Flight 2, 3 and 4, but with active control ceasing at 4.5 seconds into the simulation. We test two types of release of control, a) “Frozen”, where we hold the control surfaces at the values as set by the control system immediately before its deactivation, and b) “Zeroed”, where the control surfaces are set to their zero, or trim position. Since this is a simulation, the trim positions are perfect, resulting in zero induced roll/pitch rates. Even with these idealized conditions, the aircraft inevitably crashes within a few seconds of ceasing active control and the trajectory ceases to resemble that of the controlled case, for all tested cases.

6 Ground Truth Comparison

Due to the lack of reliability of our inertial system during these flights we have made manual measurements of the visual horizon for comparison.

6.1 Manual Horizon Selection

Measurements were made for every tenth frame of the entire video from Flight 2 which ran for over four minutes, leading to manual analysis of 777 video frames. Higher resolution images (1200x600) were used for point selection to reduce the angular error of selection to 0.25° per pixel. An average of nine image points were selected in each frame, evenly spaced along the horizon, and a least-squares fit of a planar surface was made to the corresponding unit view sphere vectors. Fig. 12 shows an example of the manual point selection and the fitted horizon. Within this image the manually selected horizon attitude gives a roll and pitch of -18.5° and 8.2° , whereas the automatic visual horizon measured -18.6° and 9.4° . Plots of the attitude for the entire of Flight 2 are shown in Fig. 13.

6.2 Visual Horizon Planarity

The main assumption made by this system is that the attitude of the aircraft can be measured by fitting a planar surface to the visual horizon line. This is independent of whether or not we require a reference that is similar to gravity, but planarity of the visual horizon almost guarantees alignment with gravity. Fig. 14a is a histogram of the angle between the manually selected horizon points and the least-squares plane fit i.e. larger error indicates that the points lie further away from the fitted plane. If the selected points pass along a great circle in the view sphere then there will be zero error, since all fitted planes are constrained to pass through the origin. The error in the histogram is on the order of a two-pixel error in manual point selection, showing that the visual horizon is quite planar.

It is expected that there is a non-planarity in this data. Our field site is located with the Teviot mountain

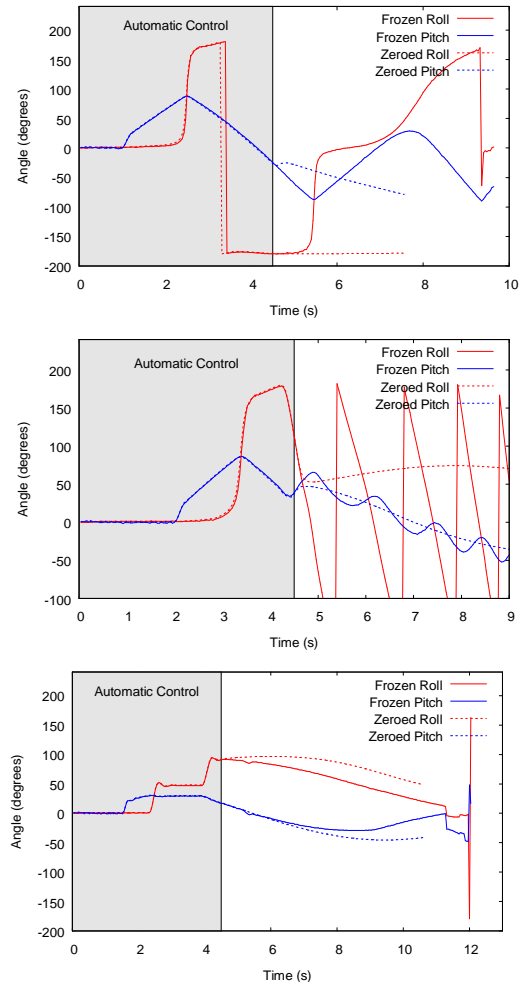


Fig. 11. Consequences of ceasing active control during maneuvers for Flight 2, 3 and 4.

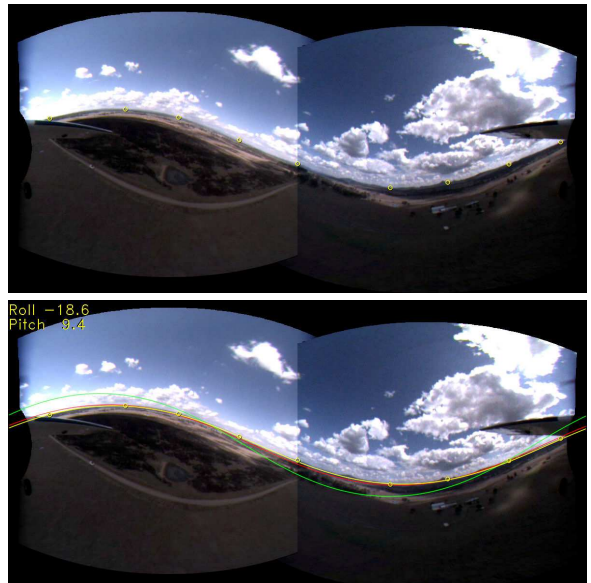


Fig. 12. Top: manual selection of horizon points indicated by small yellow circles. Bottom: the yellow line is the fit to the manually selected points, red line is the automatic visual horizon measure computed during the flight on low resolution imagery, and green line is the inertial attitude. The displayed angles are for the red line. Fine lines are drawn to show precise positions.

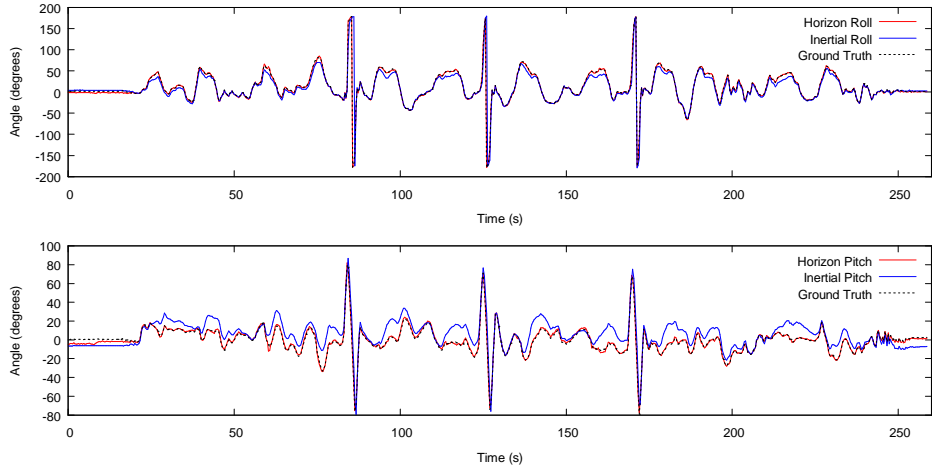


Fig. 13. Plot of attitude for the entire of Flight 2, measured every 10th frame.

range 5km to the west, and relatively flat ground to the east. The main peak on the horizon is Flinders Peak which is 679m above sea level and 12km away, while the air strip is around 50m above sea level. This mountain range should only lead to an attitude bias on the order of one degree relative to a flat earth measure.

6.3 Error Metric

If we describe each horizon measure by the vector normal to the horizon plane, then the total attitude error between two measures is the smallest angle between the two normal vectors. For example, in Fig. 12, this metric gives a total attitude error of 1.2° for the automatic visual horizon, seen as a small deviation of the red line from the yellow line.

The histogram of total attitude error for every tenth frame of Flight 2 is shown in Fig. 14b. It can be seen that 85% of automatic visual horizon measures have less than 2° error, while only 8% of the inertial measures have less than 2° error. Also, the maximum error of the automatic horizon (8.3°) is less than the median error of the inertial unit (9.1°).

This comparison is perhaps a little unfair since the automatic visual horizon is compared against a manually measured visual horizon. As stated above, the visual horizon bias for our field site should be around one degree, and we have shown that our field site horizon is near-planar and thus likely highly correlated with gravity. So, no more than a couple of degrees could have been unfairly added to the inertial error distribution.

7 Robustness to Lighting Changes

Although our system primarily uses color information for the classification of image pixels as belonging to sky or ground, it also relies partly on absolute intensity. During the flight, lighting changes dramatically as the sun comes in and goes out of view, as seen in Fig. 15. This problem is even worse for Vision System B because each camera has an independent exposure control, effectively producing two ground and two sky classes per stitched image, yet the sky/ground segmentation assumes only two classes in total.

The automatic gain control of the Firefly camera switches very quickly from one exposure level to the next. When the sun comes into full view the image jumps from

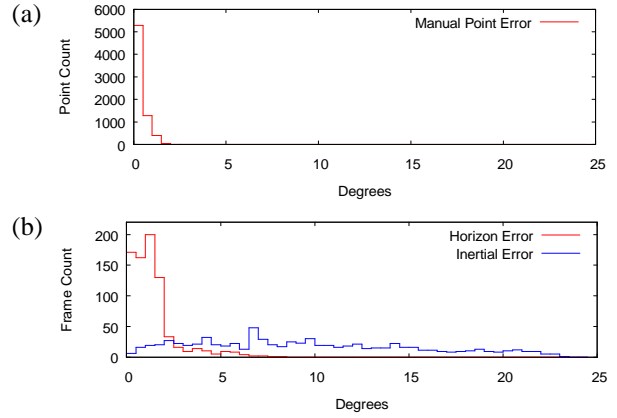


Fig. 14. (a) Histogram of angular deviation of manually selected points from the fitted plane. (b) Histogram of total attitude error of automatic horizon and inertial attitude relative to the ground truth. Each histogram bin is 0.5° wide. The total number of points is (a) 6987 and (b) 777.

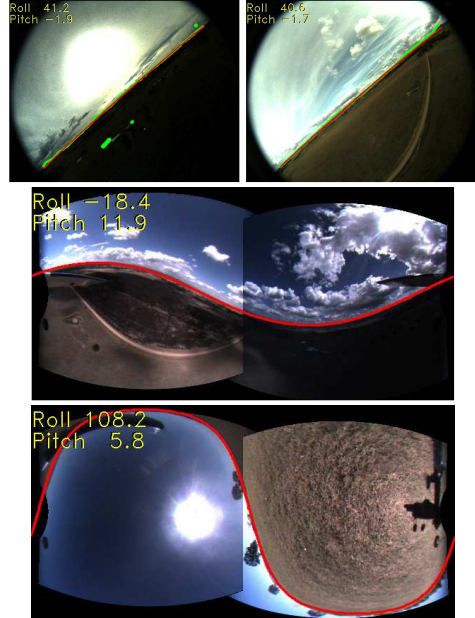


Fig. 15. Examples of lighting/exposure during flights.

a fairly even exposure across sky and ground to an exposure with a bright sky and very dark ground. Nevertheless, during these flights there was little change in the horizon-based measure of attitude over changes of exposure, lighting, and differences of cloud cover. Thus, our algorithm for sky/ground segmentation is largely immune to this problem.

The case of multiple classes of sky and ground being present for Vision System B had little effect on the attitude results. In principle, it should be possible to perform image processing separately on the left/right images and then fit the planar surface to the combined horizon points, but this was found to be unnecessary for our visual scenes. This demonstrates a useful degree of robustness in the automatic threshold technique used here.

8 Conclusion

This paper has demonstrated the feasibility of using a visually based horizon detection system to monitor and control the attitude of an aircraft, not only to stabilize flight, but also to perform extreme maneuvers. The vision-based system outperforms the inertial attitude estimates from a cheap strap-down IMU. The system is robust to lighting changes, color changes and environmental changes. It is also quick to compute, and performs well in closed-loop tests of attitude stabilization and control, providing a direct measure of attitude that is unaffected by aerobatic maneuvers. The system's ability to be integrated with any calibrated color vision system will allow it to be easily incorporated into a broad range of vision systems designed for other aspects of guidance, such as terrain following and landing. The benefits of the very wide field of view of Vision System B are evident in these maneuvers, as it allows the horizon to be reliably imaged in any aircraft attitude.

Acknowledgements

We would like to thank David Brennan for kindly allowing us to use his private air field for flight tests.

References

- [Cornall *et al.*, 2006] T. D. Cornall, A. Price, and G. K. Egan, "Measuring horizon angle on a small unmanned air vehicle using digital video camera and an FPGA," *In Proc. ICARA 2006, International Conference on Autonomous Robots and Agents*, Dec. 2006.
- [Ettinger *et al.*, 2002] S. M. Ettinger, M. C. Nechyba, P. G. Ifju, and M. Waszak, "Vision-guided flight stability and control for micro air vehicles," *Proceedings IEEE International Conference on Intelligent Robots and Systems*, 2002, vol.3 2134- 2140.
- [Gwozdecki, 2001] J.A. Gwozdecki, "Aircraft attitude sensor and feedback control system," United States Patent, Number 6181989, Jan. 2001.
- [Horiuchi, 2005] T. K. Horiuchi, "A low-power visual horizon estimation chip," *Proceedings, IEEE International Symposium on Circuits and Systems (ISCAS)*, May 2005. pp 4755-4758.
- [Jalink *et al.*, 1972] A. Jalink, Jr., R. E. Davis, and J. A. Dodgen, "Conceptual design and analysis of an infrared horizon sensor with compensation for atmospheric variability," NASA Technical Note TN-D-6616, Feb. 1972.
- [Kannala and Brandt, 2006] J. Kannala and S. S. Brandt, "A generic camera model and calibration method for conventional, wide-angle, and fish-eye lenses," *IEEE Transactions on Pattern Analysis and Machine Intelligence*, 2006.
- [Merhav, 1996] S. Merhav, *Aerospace Sensor Systems and Applications*. Springer, 1996, pp. 415-426.
- [Rohac, 2005] J. Rohac, "Accelerometers and an aircraft attitude evaluation," *Proceedings IEEE Sensors Conference*, Nov. 2005.
- [Thurrowgood *et al.*, 2009] S. Thurrowgood, D. Soccol, R. J. D. Moore, D. Bland, and M. V. Srinivasan, "A vision based system for attitude estimation of UAVs", *IEEE/RSJ International Conference on Intelligent Robots and Systems*, 11-15 October, St. Louis, Missouri, USA, 2009.
- [Todorovic *et al.*, 2003] S. Todorovic, M. C. Nechyba, and P. G. Ifju, "Sky/ground modeling for autonomous MAV flight," *Proceedings IEEE International Conference on Robotics and Automation (ICRA)*, 2003, vol.1 pp. 1422-1427.